IEEE Access
Multidisciplinary ⋮ Rapid Review ⋮ Open Access Journal

Received 6 July 2022, accepted 17 August 2022, date of publication 23 August 2022, date of current version 29 August 2022.

Digital Object Identifier 10.1109/ACCESS.2022.3201127

RESEARCH ARTICLE

Integrated Solar Mesh Dipole Antenna Based Energy Harvesting System

MORSY AHMED MORSY AND KHALID SALEH
Department of Electrical Engineering, College of Engineering, Shaqra University, Al Dawadmi, Shaqra, Riyadh 11911, Saudi Arabia
Corresponding author: Morsy Ahmed Morsy (morsy_ismail@su.edu.sa)

This work was supported by the Deputyship for Research and Innovation, Ministry of Education, Saudi Arabia, under Project IFP2021-055.

ABSTRACT This paper presents a Sunlight-Radio Frequency (RF) energy harvesting system built on Solar Panel Mesh Dipole Antenna integration. The dipole antenna mesh is mounted on the surface of the solar panel at the separations between the cells. This configuration maximizes the absorption of both solar and RF energies. Further, the multiple mesh antennas are integrated vertically to increase the RF harvested power. Each antenna output is connected to a six-stage RF-Voltage Doubler Rectifier (RF-VDR) circuit to convert the RF signal to a direct current (DC) and added to the solar panel DC output. This paper involves the design analysis of the antenna parameters, the integration process, and the design of the RF matching circuit. Prototype tests show that the proposed mesh dipole antenna has 83% efficiency. This is better than earlier similar designs published. From previous designs, the measured RF to DC conversion efficiency (CE) of the VDR circuit was merely 62% when the RF input equals −14 dBm. Moreover, the solar panel efficiency has been enhanced by 41.3 % when the input RF power density equals 49.16 mW/m^2. Finally, the results proved that the proposed solar antenna system achieves 28.5 % power CE and outperforms the others that use transparent patch antennas.

INDEX TERMS Energy harvesting, solar cell, mesh dipole antenna, RF voltage doubler rectifier, conversion ratio, impedance matching, return loss, conversion efficiency.

I. INTRODUCTION

Conventional solar panels that are commercially available, have a mere efficiency value of around 19% [1]. Despite years of study and research, none has breached the 19% barrier. In the information age, the presence of radio waves e.g. has become ubiquitous in a very broad spectrum. This motivated researchers to use antennas to harvest this broad spectrum of electromagnetic energy and convert them into electrical energy to charge small batteries. However, antenna and conversion efficiency (CE) has always been capped to a low level. The research community was eventually led to investigate the integration of both solar and RF energy harvesting. Different designs of integration were attempted to improve this efficiency [2]. The design parameters were eventually reduced to antenna shape, material, size, bandwidth, and matching with the analog to direct current (DC) conversion circuit as the most important factors that must be considered to improve the overall CE of the integrated system. In the integrated solar-antenna systems, the copper antenna is placed on the top surface of the solar panel to improve the absorption of solar energy and radio frequencies to a point the total energy level exceeds the level produced by the solar panel alone. This is achieved by choosing the position of the antenna elements so that it does not interfere with the amount of solar energy absorbed by the solar cells. At the antenna output, there is a rectifier circuit that converts the AC radio frequency (RF) signal into DC throughout the day, especially when the solar cells are inactive during the night [3]. The perfect impedance matching between the antenna output and the power conversion circuit is also important to avoid signal reflection and obtain the highest possible integrated system efficiency. The main objective of any energy harvesting system is to increase its overall CE [4], [5], [6]. Therefore, the efficiency of the antennas in these systems is the essence and must be taken into consideration very carefully [7]. In the antenna

The associate editor coordinating the review of this manuscript and approving it for publication was Debdeep Sarkar.

TABLE 1. Comparison of integrated solar antenna energy harvesting system designs.

Ref. No.	No. of Cell	Frequency band (GHz)	Solar cell area (mm^2)	Antenna area (mm^2)	Type of antenna	Harvested RF power	Harvested solar power
[23]	1	2.38-2.5	150×150	150×150	Microstrip	0.34 mW @ 2.45 GHz	1.68 mW @ 360 lux
[18]	1	2.3-2.45	N.A.	N.A.	Microstrip	0.02 mW @ 2.45 GHz	0.75 mW @ 100 lux
[19]	1	1.8-2, 2.1-2.4	80×150	180×150	Microstrip	0.08 mW @ 2.29 GHz	N.A.
[20]	1	0.95-2.45	98×144	19.6×28.8	Microstrip	0.5 µW @ 2.45 GHz	27.4 mW @ 1450 lux
[21]	1	2.2-12.1	17×33.5	38×86	Microstrip	6 µW @ 2.51 GHz	N.A.
[22]	1	2.28-2.55	22.8×24	45×45	Microstrip	35 µW @ 2.45 GHz	0.07 mW @ 334 lux
Proposed work	72	0.05-0.65	25×20 per cell	25×20 per mesh	Wire mesh antenna array	311 mW @ 0.4 GHz	600 mW @ 900 lux

construction, structure resonance and material conductivity characteristics are factors that must be considered to maximize the harvest bandwidth. One of the constraints is the precise design of the energy conversion circuit, especially the matching circuit, [8], [9], [10], [11], [12], [13], [14], [15]. The circular polarized patch antennas with harmonic rejection with sufficient matching techniques succeeded to collect RF energy at multiple frequencies within a broad frequency band from 350 MHz to 2500 MHz [16], [17], [18], [19], [20], [21], [22], [23]. In these designs, it is observed that the effect of antenna position on the amount of energy harvested through the solar cells will have a minimum effect during the day. While only the antenna harvests energy during the night period. Transparent radiation structures are utilized to form antennas above the surface of solar panels so that the antennas would not affect the amount of solar energy absorbed. The summary of the previous related work performance results compared with the performance of the proposed work has been illustrated in Table 1. In most of the previous designs, the ratio between solar area and antenna area is less unity [2], [3], [4], [5], [6]. Some of these works use a transparent material to implement the antenna for increasing this ratio to unity and improve the hybrid energy harvested [1]. Wire antenna can be used to prevent the blocking of sunlight absorption and also use the total area of the solar panel to increase the harvested RF energy. One of the main reasons why earlier designs of this type are not cost-effective is the expensive transparent radiation material. Thus, one of the main objectives of this paper is to implement an integrated harvesting system of solar panels and RF antennas shown in Fig. 1 without using a transparent radiation material. Also, note that it is shown in this that the success of an integrated system for harvesting electromagnetic energy in RF and solar energy relies heavily on the low loss high gain of the RF amplifier. For this combined reason, a wire mesh dipole was designed so that we can use the separation spaces between the cells of the solar panel to embed the antenna mesh without blocking the absorption of the sun's rays. The antenna mesh was designed to resonate and harvest the ultra-high frequency (UHF) range from 0.350 GHz to 0.650 GHz. Thus, the combined power generation of the antenna mesh and the solar panels was noticeably higher than conventional solar panels. The antenna mesh was designed and tested for maximum power output and then embedded into a solar panel array that conforms to the resonant dimensions of the mesh.

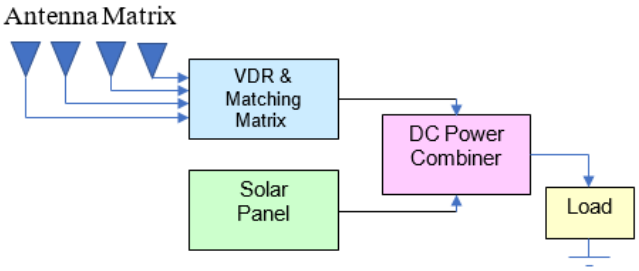

FIGURE 1. Proposed system block diagram.

The remainder of this article is organized as follows. Section II introduces the mesh dipole antenna design analysis and characteristics. Section III presents the design analysis of the energy conversion circuit and matching mechanism with the proposed antenna. Section IV is the overall system integration procedure. Section V System measurements and discussions.

II. MESH ANTENNA DESIGN AND MEASUREMENTS

A UHF wire-mesh dipole antenna design was analyzed. The design took the antenna weight, installation, disassembly, and durability into consideration. The proposed antenna is a flat planar dipole constructed from two rectangular wire mesh elements shown in Fig. 2. Table 2 illustrates the implemented and simulated antenna dimensions according to the commercial dimensions in the UHF range [8]. To reduce the simulation complexity and running time, the wire-mesh dipole simulation model is performed using the solid radiator equivalent model [8]. The mesh size was chosen according to the commercial mesh cell dimension and choice the solar panel with the same dimensions to save the absorption

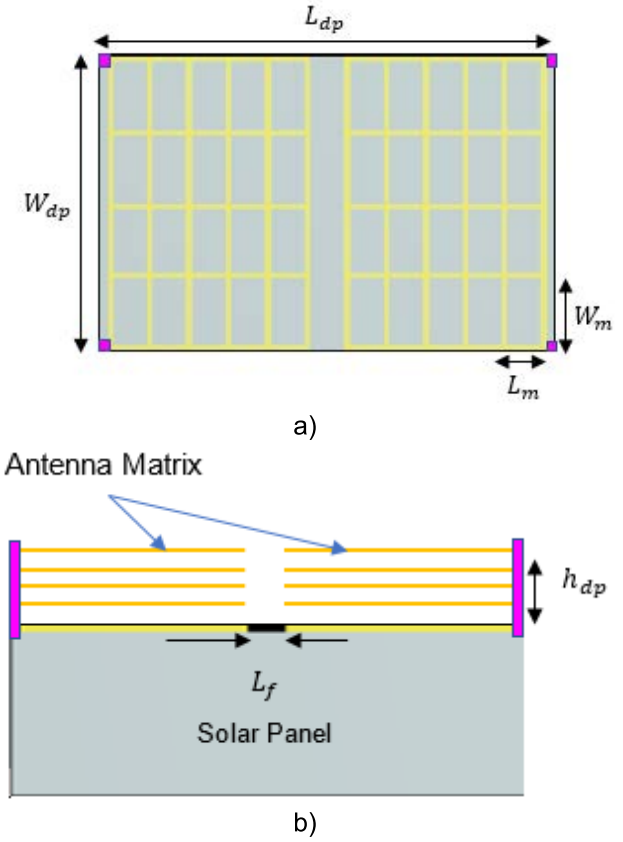

FIGURE 2. Proposed antenna model: a) Top view and b) Side view.

TABLE 2. Proposed antenna parameters.

No.	Parameter	Description	Value
1	L_{dp}	Length of dipole	35 cm
2	W_{dp}	Width of dipole	24 cm
3	h_{dp}	Hight above the solar panel	2 cm
4	L_m	Mesh cell length	2.5 cm
5	W_m	Mesh cell width	2 cm
6	Φ_m	Wire diameter	1.5 mm
7	L_f	Feeding width	3 mm
8	ε_r	Background relative permittivity	1.00

of the cells. In the design, the mesh cell dimension is in the range of the commercially available mesh size equal to 50 mm × 40 mm. In this range, the RMS error between the solid radiator reflection coefficient and mesh is 10% [8]. As a modification, the proposed antenna model has a mesh size equal to another commercially available solar panel cell size equal to 25 mm × 20 mm. The dipole length has to be 35 cm which corresponds to the one half-wavelength of the UHF scale in free space.

Figure 3 shows the measured and simulated linear, average, and normalized radiation patterns in the horizontal plane of the proposed mesh dipole antenna that consists of 72 elements. The antenna is placed 1 meter away from the Yagi-Uda antenna array as a UHF source. The power meter is connected to the mesh antenna output during a 50 Ω copper SMA

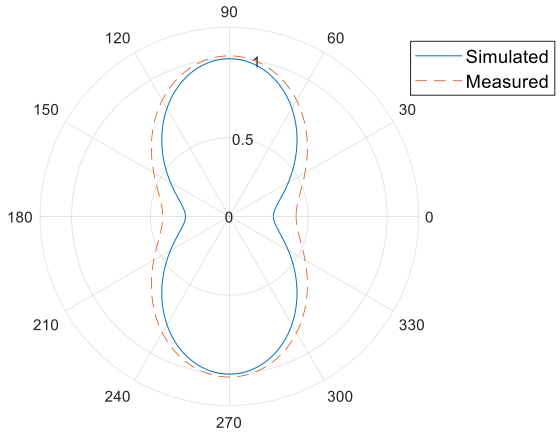

FIGURE 3. Elements mesh dipole antenna normalized radiation pattern.

connector, the proposed antenna is rotated around the source antenna and the power is measured every 15^0. The results illustrate that the half-power beamwidth of the radiation pattern measured is wider than the one simulated by approximately 6 degrees. The simulated radiation pattern has been plotted by the data matrix output from the finite difference time domain simulation tools using MATLAB. The actually measured radiation pattern has unsmoothed reading values and the plotted curve is the average of these values to can compare it simply with the simulated pattern. Additionally, Fig. 4 represents the measured and simulated return loss in dB of the proposed mesh antenna model. The results indicate that the average value of the simulated return loss of this antenna is equal to −22.5 dB in the frequency range from 350 MHz to 600 MHz, while the average value of the measured return loss in the same frequency range is −18 dB.

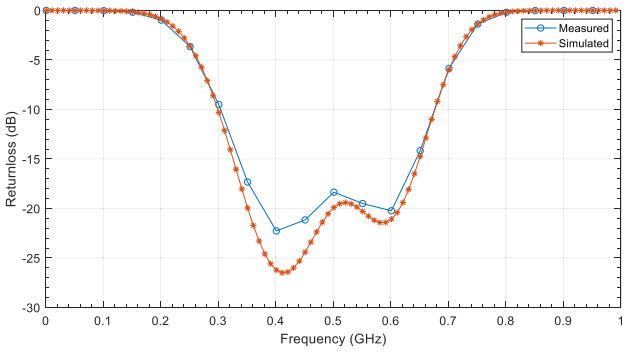

FIGURE 4. Mesh antenna return loss.

Furthermore, the optimum values of the simulated and measured return loss are equal to −27 dB and −22.5 dB respectively, at 410 MHz. Moreover, the measured radiation and total efficiency of the antenna are equal to 88% and 83% respectively.

III. MATCHING AND RF-VDR CIRCUIT DESIGN

Figure 5 illustrates the matching Thevenin equivalent circuit which is connected with the RF voltage source V_S in series with a small resistance R. While the complex load

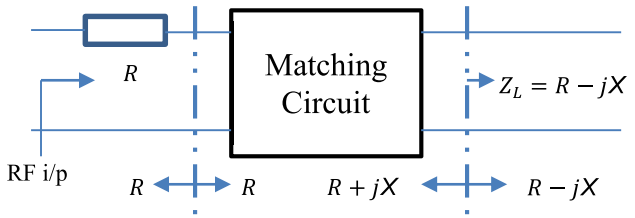

FIGURE 5. Matching circuit representation.

impedance Z_L represents the RF-VDR circuit. The maximum power delivered to the load is achieved when the VDR input impedance equals the complex conjugate of the antenna output impedance. The matching circuit was utilized to satisfy this condition. Different techniques can be used for impedance matching, such as the shunt inductor, the transformer, the π-Network, the T-Network, the LC circuit, and the transmission line.

In the proposed system, a minimum size and low cost third-order Chebyshev LC matching circuit was used in order to achieve good matching between the 50 Ω proposed mesh antenna and the RF-VDR input impedance [7]. This circuit acts as a band-pass filter operating in the frequency band form (20 – 500) MHz. The Smith chart was used to design the circuit in order to display the behavior of RF parameters in the operating frequency range.

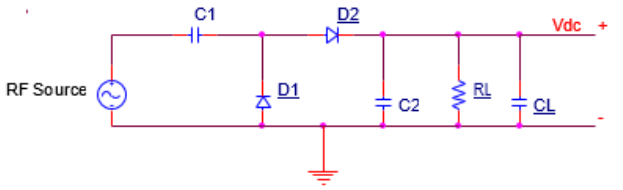

FIGURE 6. Single-stage VDR circuit [1].

Figure 6 represents a single-stage RF-VDR circuit followed by a low-pass filter which is represented by the RC parallel load. The circuit consists of two RF Schottky diodes to rectify the RF input and two capacitors to duplicate the RF peak value. The RF Schottky diode used is an HSMS2850 which is characterized by a very fast switching speed and zero biasing [14], [16], [24]. Additionally, this circuit was tested in the frequency range mentioned above and the result indicates that the DC output voltage was approximately equal to 760 mV and the DC output power was equal to 2.74 mW at 400 MHz when R_L equal to 100 KΩ.

Furthermore, to increase the DC output power, the multi-stage VDR circuit was used [7]. In the literature, many of the results found that a 7-stages VDR circuit is recommended to provide 5 V DC on 100 KΩ load resistance. In this study, the 6-stage VDR circuit shown in Fig. 7 was implemented using the components illustrated in Table 3. This circuit produces 3.7 V DC at the optimum DC output power of 78 mW, and a DC load current of 43.3 mA when the load resistance is equal to 81.1 KΩ.

TABLE 3. 6-stage vdr circuit components.

Label	Name	Value
C_1-C_{12}	Stage Capacitor	3.3 nF
D_1-D_{12}	Stage Diode	HSMS2850
R_L	Load Resistance	81.1 KΩ
C_L	Load Capacitance	100 nF

IV. OVERALL SYSTEM INTEGRATION

The slot geometry array around cells and the optically transparent patch array above the cells give very low DC output power compared with the solar panel outputs [9]. The overall efficiency of this integrated system does not exceed 21.5%, this is because the strip antenna does not harvest higher power compared to the wire and aperture antennas. Fig. 8 and Fig. 9 show the solar mesh dipole antenna integrated model and its experimental setup respectively. The proposed mesh antenna resonant dimensions conform to solar panels that already exist in the market. This panel has 12 × 6 cells and each cell has 2.5 × 2 cm^2. Each antenna cell has a length of 2.5 cm and a width of 2 cm with an overall dipole length of 35 cm and a width of 24 cm. In addition, the used copper wire is characterized by 1.5 mm diameter and 5.7×10^7 S/m conductivity. Most of the research focuses on the small-scale integrated solar antenna systems using low-power solar cells and microstrip antennas for low-power applications like; sensors, smart devices, and earphones. The proposed model in this paper is a minimum prototype of a large-scale integrated solar antenna system that can be maximized to use in the high-power applications of solar panels like; lighting, transportation, and battery charging.

One of the most important factors that were taken into account when designing the antenna, was that it should be in the spaces between the cells so as not to affect the amount of light absorption by the solar panels. Thus, improving efficiency. There was more than one prototype antenna built and placed vertically with a 3 mm spacing between them to harvest the largest possible amount of energy. Then add this to the output energy of the solar panel so that the overall power output of the system gains significant improvement or increase compared to that of the conventional solar panel. Note that by configuring the antenna as a vertical mesh, it provided additional reflection back towards the solar cells. This provides for the sunlight initially reflected from the surface of the solar cell, instead of being absorbed. This is considered one of the inefficiencies of available solar panels. This effect is similar to trapping layers used in nano cells. The mechanism of light reflection is illustrated in Fig. 10. This figure shows that when an incident ray (no. 1) hits the solar cell surface, not all of this energy is absorbed by the solar cell as normally assumed. In reality, most of the energy is reflected (no. 2). With the vertical mesh antenna in place, the reflected light energy (no. 2) from the solar cells is reflected (no. 3) to the solar cell surface resulting in an increased rate of solar energy absorption for every incident of sunlight. To create the vertical antenna matrix above the solar panel surface, the material with high reflectance is used.

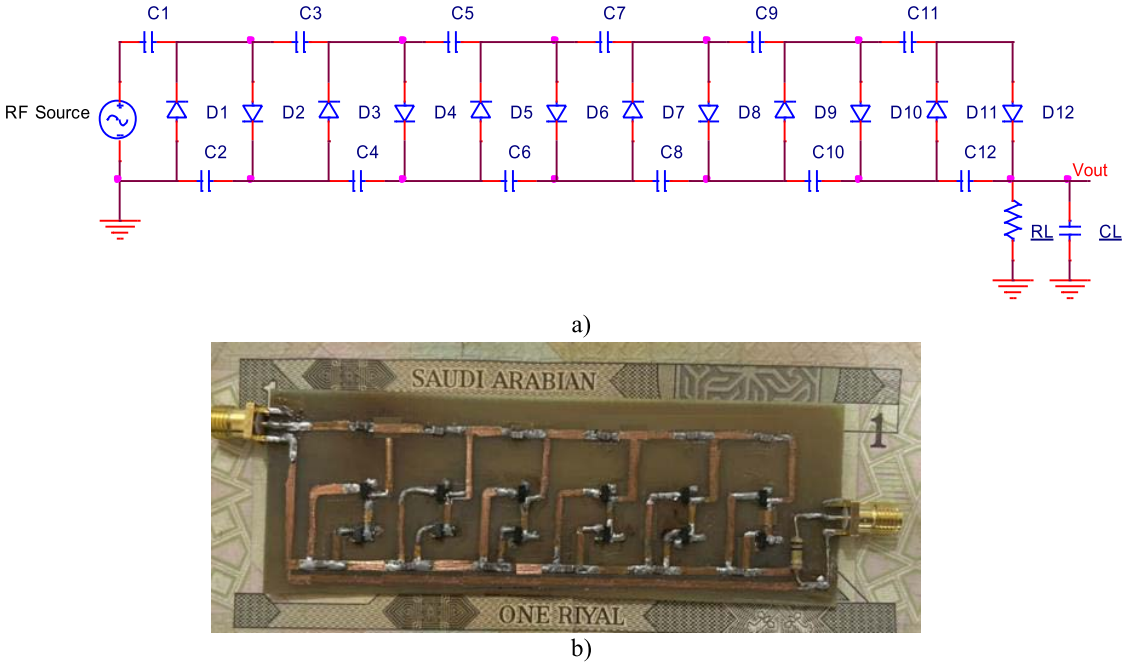

FIGURE 7. The proposed 6-Stage RF-VDR a) circuit diagram and b) practical implementation.

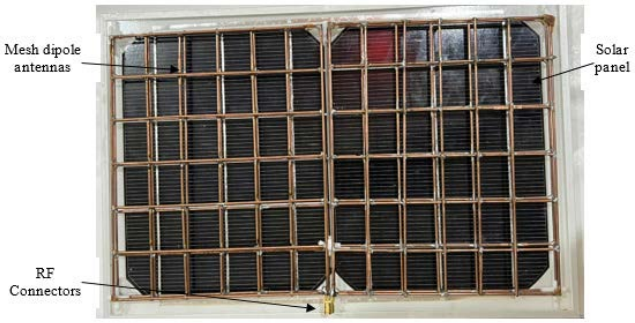

FIGURE 8. The practical model of integrated soar 4-mesh dipole antenna system.

This material can be exploited to reflect some of the reflected sunlight rays from the surface of the solar panel to this surface again at different angles, which can help the solar panel to absorb it.

This is an additional improvement of the presence of antennas on the solar cell surface.

Figure 11 represents the overall system equivalent circuit of the system combiner mentioned before in Fig. 1. This consists of a solar DC output V_{Solar} and four additional DC outputs that represent the outputs of the VDR circuit matrix. For m matrix dimensions the total DC output is stated as:

$$V_{Total} = V_{Solar} + V_{DC.1} + V_{dc.2} + \ldots + V_{DC.m} \quad (1)$$

assuming identical antenna and VDR circuits we can assume that $V_{DC} = V_{DC.1} = V_{DC.2} = V_{DC.3} = \ldots = V_{DC.m}$ and equation (1) can be rewritten as:

$$V_{Total} = V_{Solar} + mV_{DC} \quad (2)$$

Additionally, the total output power can be expressed as:

$$P_{Total} = P_{Solar} + mV_{DC} * I_{Load} \quad (3)$$

The RF to DC CE is measured when adjusting the source antenna on the maximum output power that gives 49.16 mW/m^2 power density at the surface of the proposed antenna. Firstly, measuring the RF output power at the output of the proposed antenna. Connect the proposed antenna output to the RF-VDR circuit through the matching circuit and measure the DC output power of this circuit. Combine the output of the four antennas followed by four RF-VDRCs and measure the overall DC output power then use (4) to calculate the RF to DC CE of the combined system [7].

$$CE_{RF-DC} = \frac{DC\ output\ power\ from\ the\ four\ mesh\ antenna}{RF\ input\ power\ to\ the\ RF-VDR\ circuit} \quad (4)$$

The total output power obtained from this system ranges between 723 mW to 901 mW according to the number of antenna are used. While, the corresponding load current I_{Load} ranges from 38.8 mA to 43.3 mA at the optimum load resistance of 480 Ω.

All results were taken with a normal incident white light source and a maximum output of 6 V and 0.6 W from the solar panel. At this stage, we can calculate the maximum CE achieved from the proposed system using the solar panel data sheet and measured values. The data sheet shows that the solar panel's maximum output power at 6 V DC output, open-circuit voltage, is 0.6 W. These values are at 19 % optimum CE. The added power by the proposed antenna integration is 0.311 W.

The resulting maximum output power from the proposed system is, therefore, 0.901 W giving an approximate 28.5%

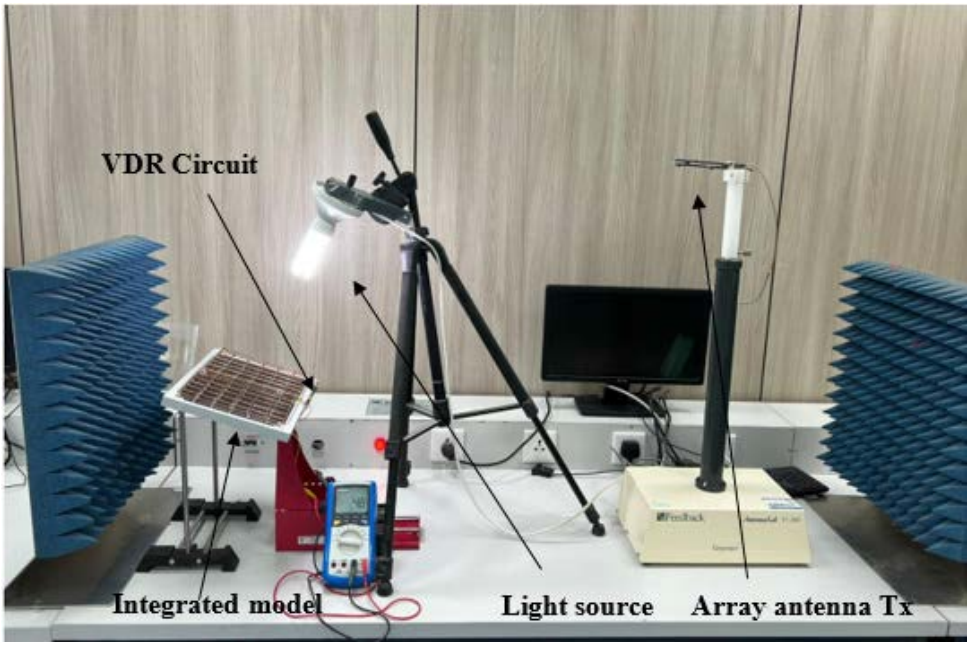

FIGURE 9. Integrated system experimental setup.

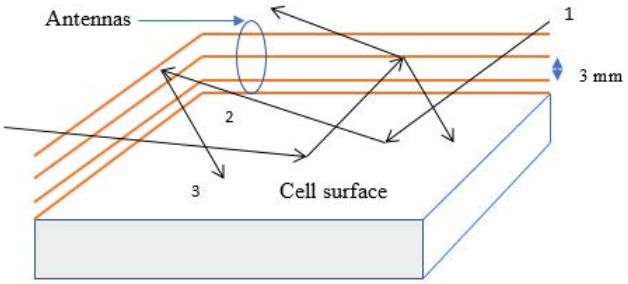

FIGURE 10. Effect of the antenna on the reflected rays from the cell surface.

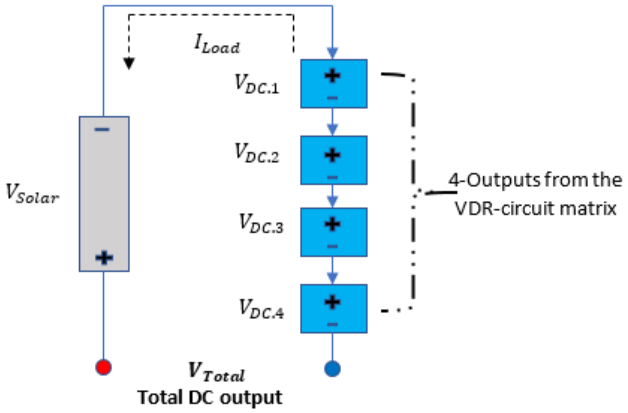

FIGURE 11. System equivalent circuit.

CE. However, there is an obvious physical limitation to the proposed system. If the number of mesh antennas exceeds four, the overall output power gain starts to decrease due to the increased blocking of the light from the Sun to the solar panel. For this reason, four is the optimal number of antennas that can be mounted on top of the solar panel. The normal range of the received UHF power density is from 30 to 100 mW/m^2[13]. This depends on the following factors: the alignment between the transmitting and receiving antennas, the distance separation between them, and the size of the receiving antenna. The RF beamforming technique can be used to maximize the output power from the antenna and improve the overall power CE of the system. In this paper, the used UHF source is placed 1 meter away from the proposed mesh dipole antenna and provides 49.16 mW/m^2 at the surface of the solar panel.

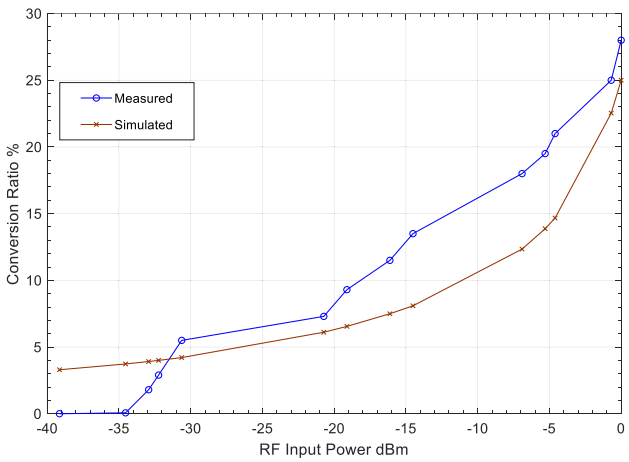

FIGURE 12. 6-stage VDR circuit conversion ratio versus the RF input power.

V. MEASUREMENT AND DISCUSSIONS

Theoretically, the conversion ratio has a value at any value of the input RF power because it's represented by the

mathematical model. In reality, however, circuit sensitivity plays a big role in measuring the voltage conversion ratio. Fig. 12 illustrates a comparison between the measured and simulated RF-VDR circuit voltage conversion ratio. Connect the input of the RF-VDR circuit to the RF source and vary the power level from −40 dBm to 0 dBm and take different reading at the output of the circuit then use (5) to calculate the circuit conversion ratio in %.

$$conversion\ ratio = \frac{the\ output\ of\ the\ RF - VDRinwatt}{the\ input\ of\ the\ RF - VDRinwatt} \tag{5}$$

The result shows that when the input power is less than or equal to −35 dBm, the measured output power is 0 dBm as well as 0% voltage conversion ratio, but the simulated conversion ratio value is just below 5. When the input power exceeds −35 dBm, the measured voltage conversion ratio is increased with a low average slope of approximately 4% per decade up to −20 dBm. This is due to circuit losses. Further, when the input power exceeds −20 dBm, up to 0 dBm, the average voltage conversion ratio is approximately 20%.

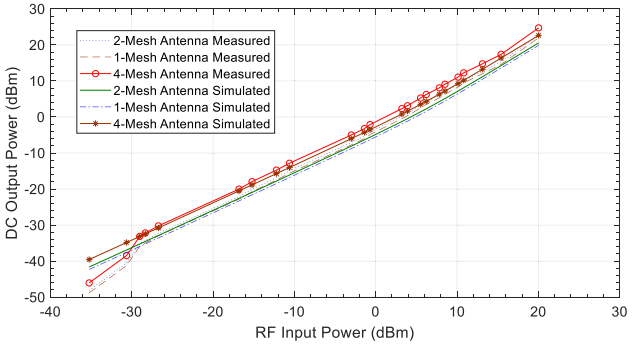

FIGURE 13. DC output power versus the RF input power for a different number of mesh dipole antenna above the cell surface at 5 mm separation.

Figure 13 shows the measured and simulated DC output power versus the RF input power for a different number of a mesh dipole antenna mounted on top of the solar cell surface with a 5 mm distance separation. The result illustrates that when the input RF power is above −30 dBm the measured and simulated results are approximately the same for 1 and 2 mesh antenna-solar panel integration but differ for 4-mesh antenna integration. This difference appears when the input power exceeds −17 dBm. At 0 dBm RF input power, the measured output DC output power is approximately −4 dBm for 1 mesh, −3 dBm for 2 mesh, and −1 dBm for 4 mesh antenna integration. This result means that when the number of antennas increases beyond 4, the output harvested power increase but does not exceed the input power because the losses of the antenna and VDR circuit is comparable to the input RF power. While, when the input power exceeds 10 dBm, the measured and simulated DC output power are exceeding the input power with the 4-antenna mesh and Solar panel integration.

The light source used in the measurement setup is characterized by 100 W/900 LM, and provides 31.85 W/m^2 directed perpendicularly to the surface of the solar panel. This power density is enough to reach the DC output power of the solar panel to the maximum value of 0.6 W according to its datasheet. When the light source is switched off, the measured DC output power from the combined four RF-VDR equals 0.311 W. These results indicate that the measured DC power value collected from a 4-mesh antenna is 12 dBm at 10 dBm RF input power, and 25 dBm at 20 dBm RF input power. This translates to 300 mW for each antenna at 100 mW RF input power. 300 mW is approximately half the value of the solar panel DC output power. The total combined DC power from the panel and antenna is equal to 0.9 W from 0.911 W at the combiner input which represents 98.8% DC combining efficiency and 28.5 % system power conversion efficiency compared to 19 % by a conventional solar panel itself. The measured angular performance of the proposed integrated solar-antenna system is shown in Fig. 14. This is in comparison with the measured angular performance of the solar panel itself. The behavior of the two results is approximately the same because most of the power output is from the solar panel and a little from the mesh antenna. This indicates that the difference between the two results varies with the angle. Inversely, decreasing as the angle changes from 0^0 to 90^0. At 0^0 the CE of the integrated solar antenna system is at 8 % while at 90^0 the difference is decreased to 2%. This 2 % is due to the surrounded UHF waves around the antenna matrix and the remaining 6 % is due to the antenna polarization.

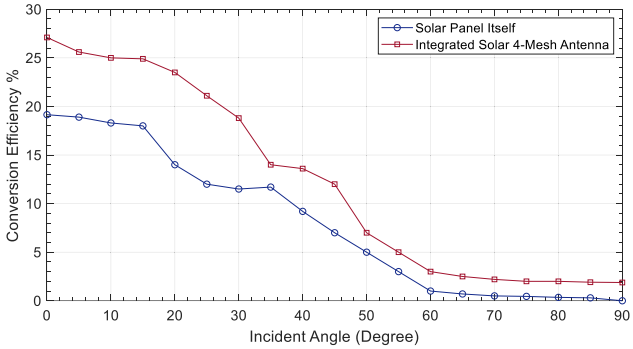

FIGURE 14. Measured angular performance of the solar panel itself compared with the integrated solar 4-mesh dipole antenna system.

Further, at angle 30^0 the integrated system performance is equal to the performance of the solar panel itself at angle 0^0. This means that the performance of the proposed system is reduced to 70.3 % from the maximum. While the performance of the solar panel itself is reduced to 63 % from the maximum.

VI. CONCLUSION

In this study, an innovative energy harvesting system based on a commercial solar panel and novel rectangular mesh dipole wire antenna has been proposed and analyzed.

The proposed mesh antenna was designed based on the solar panel dimensions and separations between cells. Further, a six-stage RF-VDR circuit was implemented to convert the RF output from the antenna into DC power and added to the solar power output. This antenna is resonant to the UHF range with 35 cm × 24 cm actual dipole dimensions, 2.5 cm × 2 cm mesh size, 0.15 cm wire diameter, 5.7×10^7 S/m wire conductivity, and 72 elements. An antenna matrix of 4 mesh dipole was placed above the solar panel surface to increase the RF energy harvested and confinement of the reflected light rays from the solar surface. The overall system integration and all performance parameters were measured. All the measured parameters are compared with the simulated ones and discussed. The most important result is the enhancement of the overall system conversion efficiency, the proposed system provides 28.5 % power CE representing a 9.5% or 41.3 % enhancement over the power CE of the solar panel itself.

REFERENCES

[1] Y. Zhang, S. Shen, C. Y. Chiu, and R. Murch, "Hybrid RF-solar energy harvesting systems utilizing transparent multiport micromeshed antennas," *IEEE Trans. Microw. Theory Techn.*, vol. 67, no. 11, pp. 4534–4546, Nov. 2019, doi: 10.1109/TMTT.2019.2930507.

[2] J. Bito, R. Bahr, J. G. Hester, S. A. Nauroze, A. Georgiadis, and M. M. Tentzeris, "A novel solar and electromagnetic energy harvesting system with a 3-D printed package for energy efficient Internet-of-Things wireless sensors," *IEEE Trans. Microw. Theory Techn.*, vol. 65, no. 5, pp. 1831–1842, May 2017.

[3] T. Peter, T. A. Rahman, S. W. Cheung, R. Nilavalan, H. F. Abutarboush, and A. Vilches, "A novel transparent UWB antenna for photovoltaic solar panel integration and RF energy harvesting," *IEEE Trans. Antennas Propag.*, vol. 62, no. 4, pp. 1844–1853, Apr. 2014.

[4] O. O'Conchubhair, K. Yang, P. McEvoy, and M. J. Ammann, "Amorphous silicon solar Vivaldi antenna," *IEEE Antennas Wireless Propag. Lett.*, vol. 15, pp. 893–896, 2016.

[5] Y. Tawk, J. Costantine, F. Ayoub, and C. G. Christodoulou, "A communicating antenna array with a dual-energy harvesting functionality [wireless corner]," *IEEE Antennas Propag. Mag.*, vol. 60, no. 2, pp. 132–144, Apr. 2018.

[6] K. Niotaki, F. Giuppi, A. Georgiadis, and A. Collado, "Solar/EM energy harvester for autonomous operation of a monitoring sensor platform," *Wireless Power Transf.*, vol. 1, no. 1, pp. 44–50, Mar. 2014.

[7] M. Morsy and O. Galal, "Optimized triple-band h-shaped slot microstrip antenna array based wireless mobile charger," *Int. J. Commun. Antenna Propag.*, vol. 11, no. 1, pp. 49–56, 2021, doi: 10.15866/irecap.v11i1.20072.

[8] Z. Lei, "Radiation pattern analysis of reflector antennas using CAD model-based physical optics method," *IEEE Access*, vol. 7, pp. 162598–162604, 2019, doi: 10.1109/ACCESS.2019.2952222.

[9] W. An, S. Xu, F. Yang, and J. Gao, "A Ka-band reflectarray antenna integrated with solar cells," *IEEE Trans. Antennas Propag.*, vol. 62, no. 11, pp. 5539–5546, Nov. 2014, doi: 10.1109/TAP.2014.2354424.

[10] W. An, L. Xiong, S. Xu, F. Yang, H.-P. Fu, and J.-G. Ma, "A Ka-band high-efficiency transparent reflectarray antenna integrated with solar cells," *IEEE Access*, vol. 6, pp. 60843–60851, 2018, doi: 10.1109/ACCESS.2018.2875359.

[11] M. A. Morsy and K. Saleh, "Efficiency enhancement of GaAs nano solar cell based on 2D photonic crystal trapping layer and 2D index modulation layer," *IEEE Access*, vol. 10, pp. 44147–44158, 2022, doi: 10.1109/ACCESS.2022.3169414.

[12] F. M. E. Nashad, S. Foti, D. Smith, M. Elsdon, and O. Yurduseven, "Ku-band suspended meshed patch antenna integrated with solar cells for remote area applications," *Prog. Electromagn. Res. C*, vol. 83, pp. 245–254, 2018.

[13] S. Yu, S. Lee, H. Lee, and Y. B. Park, "Study of mesh pattern for optically transparent flexible antenna with feedline," *Appl. Sci.*, vol. 11, no. 21, p. 10002, Oct. 2021, doi: 10.3390/app112110002.

[14] T. Alam, M. T. Islam, M. A. Ullah, R. Rahmatillah, K. Aheieva, C. C. Lap, and M. Cho, "Design and compatibility analysis of a solar panel integrated UHF antenna for nanosatellite space mission," *PLoS ONE*, vol. 13, no. 11, Nov. 2018, Art. no. e0205587, doi: 10.1371/journal.pone.0205587.

[15] V. Akan and E. Yazgan, "Antennas for space applications: A review," in *Advanced Radio Frequency Antennas for Modern Communication and Medical Systems*, A. Sabban, Ed. London, U.K.: IntechOpen, 2020, doi: 10.5772/intechopen.93116.

[16] E. Wahjono, D. Anggriawan, E. Sunarno, S. Nugraha, and A. Tjahjono, "Maximum power point tracking of photovoltaic module for battery charging based on modified particle swarm optimization," *Int. Rev. Model. Simulations*, vol. 10, no. 1, pp. 77–84, 2017.

[17] J. Fanton, "Wireless power transmission: State of the art and perspectives," *Int. Rev. Electr. Eng.*, vol. 14, no. 3, pp. 205–219, 2019.

[18] Y. Ahmed, S. Mohideen, T. Ali, and P. Manohara, "A planar inverted-F antenna (PIFA) loaded with slot for RF energy harvesting application," *Int. J. Commun. Antenna Propag.*, vol. 10, no. 1, pp. 51–57, 2020.

[19] S. Ahmed, Z. Zakaria, M. Husain, and A. Alhegazi, "A novel design of circularly polarized aperture-coupled antenna with harmonic rejection for rectenna application," *Int. J. Commun. Antenna Propag.*, vol. 8, no. 4, pp. 288–293, 2018.

[20] E. M. Ali, N. Z. Yahaya, N. Perumal, and M. A. Zakariya, "Design of microstrip patch antenna at 900 MHz for charging mobile applications," *J. Eng. Appl. Sci.*, vol. 12, no. 4, pp. 988–993, 2017.

[21] T. Sanislav, S. Zeadally, G. D. Mois, and S. C. Folea, "Wireless energy harvesting: Empirical results and practical considerations for Internet of Things," *J. Netw. Comput. Appl.*, vol. 121, pp. 149–158, Nov. 2018.

[22] F. Z. Khoutar, M. Aznabet, and O. E. Mrabet, "Gain and directivity enhancement of a rectangular microstrip patch antenna using a single layer metamaterial superstrate," in *Proc. 6th Int. Conf. Multimedia Comput. Syst. (ICMCS)*, May 2018, pp. 1–4.

[23] S. Gnanamurugan, B. Narmdha, A. Shamina, and M. Sindhu, "Gain and directivity enhancement of rectangular microstrip patch antenna using HFSS," *Asian J. Appl. Sci. Technol.*, vol. 1, pp. 1–6, Mar. 2017.

[24] K. B. Bondili and G. Immadi, "Design and analysis of high gain linear rectangular microstrip array antenna at 20.2 GHz of Ka band," *Wireless Pers. Commun.*, vol. 111, no. 3, pp. 1563–1573, Apr. 2020.

MORSY AHMED MORSY was born in Cairo, Egypt, in 1979. He received the B.Sc., M.Sc., and Ph.D. degrees from the Faculty of Engineering, Ain Shams University, Cairo, in 2000, 2007, and 2013, respectively. He is currently an Assistant Professor in analog and digital communication, antennas and wave propagation, and optical fiber communications with the Electrical Engineering Department, College of Engineering, Shaqra University, Riyadh, Saudi Arabia. He has published 17 journals and conference papers. His research interests include optical communications, free space optics, visible light communications, photonics, 2-D-photonic crystals, RF energy harvesting systems, optical communication networks, and solar antenna integration. He was a member of the ABET and NCAAA teams.

KHALID SALEH received the bachelor's degree in electrical engineering from King Saud University, Riyadh, Saudi Arabia, in 2006, the master's degree in electrical engineering from the University of Colorado, Denver, CO, USA, in 2010, and the Ph.D. degree from Arizona State University, Tempe, AZ, USA, in 2017. He has taught various courses, such as automatic control systems, digital control systems, and electric circuits. He is currently the Dean of the College of Engineering, Shaqra University, Al Duwadimi, Saudi Arabia. His research interests include applied mathematics, fractional order systems, signals analysis, digital image processing, linear and nonlinear systems analysis, and digital control systems.